UCRL-95598
PREPRINT

A Wideband Spectrograph for Free Electron Laser Experiments

B. Kulke, M.J. Burns, T.J. Orzechowski

This Paper was Prepared for Submittal to
Review of Scientific Instruments

July 10, 1986

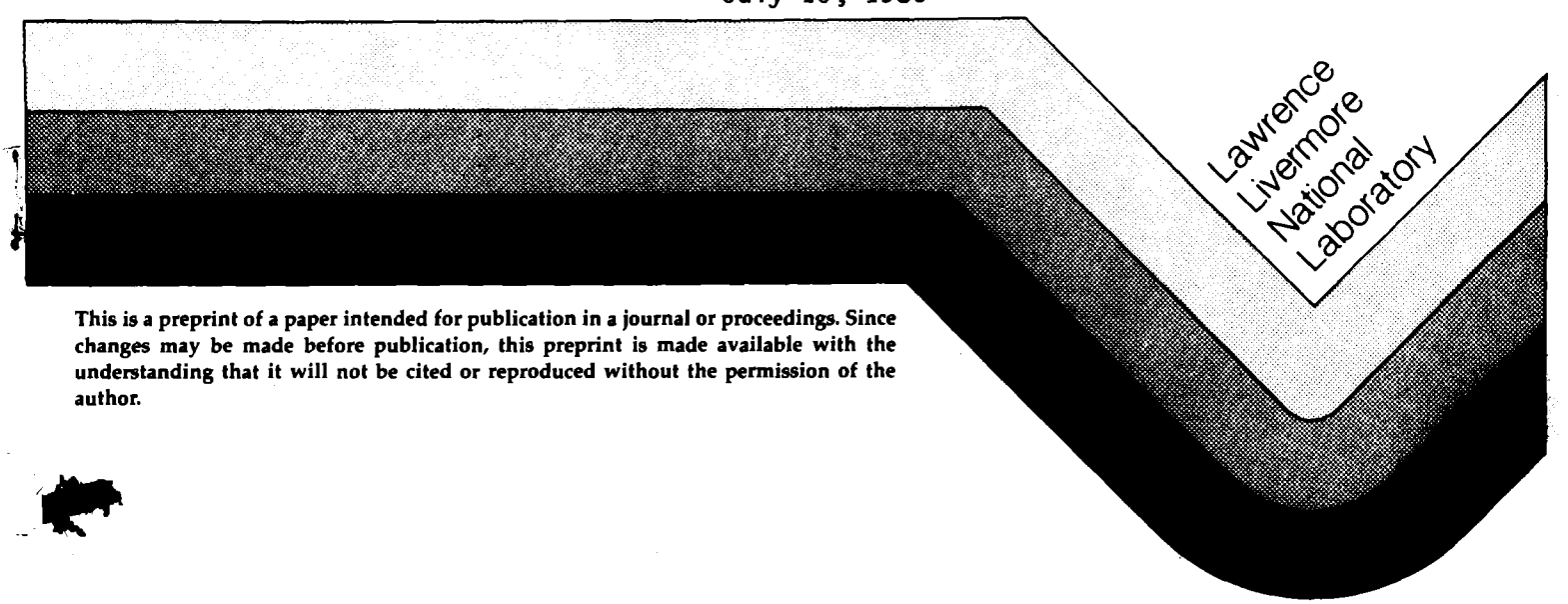

DISCLAIMER

A WIDEBAND SPECTROGRAPH FOR FREE ELECTRON LASER EXPERIMENTS

B. Kulke, M. J. Burns, and T. J. Orzechowski
Lawrence Livermore National Laboratory*
Livermore, CA 94550

July 10, 1986

ABSTRACT

We have designed, calibrated, and deployed an electron spectrograph to measure the effect of the free-electron laser interaction on the relativistic electron beam in an FEL. The spectrograph spans a wide energy range ($\Delta E/E > 1$) and is designed for electron energies from 2 to 4 MeV.

*Performed jointly under the auspices of the U.S. Department of Energy by Lawrence Livermore National Laboratory under W-7405-ENG-48 and for the Department of Defense under SDIO/BMD/ATC MIPR No. W3-RPD-53-A127.

A WIDEBAND SPECTROGRAPH FOR FREE ELECTRON LASER EXPERIMENTS

B. Kulke, M. J. Burns, and T. J. Orzechowski
Lawrence Livermore National Laboratory*
Livermore, California 94550

INTRODUCTION

The free electron laser facility (ELF) at LLNL utilizes a nominal 1 kA, 3-4 MeV beam to generate hundreds of kilowatts of 35 GHz microwave power.[1] It is of interest to measure the energy spectrum of the electron beam both with and without the microwave interaction, by means of a spectrograph placed directly downstream from the wiggler magnet. The design and construction of a Brown-Buechner type of spectrograph for a similar purpose, with a 20% energy range, was described recently by Kennedy and Adamski.[2] The present note discusses the design and performance of an Elbek spectrograph.[3,4] This instrument is a 110 degree spectrograph, with unusual poleface rotation angles that provide exceptional second-order correction, i.e., good focusing of an incoming beam sample with large angular divergence, over a relatively wide energy range.

ELECTRON OPTICS DESIGN

A plan view of the basic geometry is given in Fig. 1, showing the effective magnetic field boundaries and the extreme trajectories of the entering ray

bundles. The purpose of the protruding "nose" is to simulate a wide symmetrical pole edge for the entering beam sample which would otherwise enter at a corner. The energy range of this instrument is 2-4 MeV. For design purposes, the source was assumed to be a 3A, 1mm dia sample of the 1 kA, 50 ns, pulsed, ELF electron beam as it emerges from the wiggler magnet. At this point that beam is assumed to have a 1-cm radius and a 400 mr-cm normalized emmittance; consequently, the half angle of the conical sample beamlet will vary from 83 mr at 2 MeV to 46 mr at 4 MeV. The design further places a quadrupole singlet (gradient 1.42 kG) between the source point and the dipole magnet. This provides vertical prefocusing of the expanding beamlet to get good transmission through the dipole region; more vertical focusing is achieved by the 35 degree rotation of the entry pole face. (In actual use, the quadrupole turned out to be of marginal benefit and was later removed). The central rays are turned through 110 degrees in going from entrance to exit pole face. The latter has a negative rotation angle of 35 degrees, and essential feature of this design, based on the calculations by Borggren, Elbek, and Nielson.[3]

In order to reduce the spatial extent of the fringe field, the dipole magnet was designed for the minimum gap width (20 mm) consistent with allowing room for the vacuum chamber. The effective clearance height for the beam is just under 12 mm. The nominal dipole field was chosen at 1 kGauss, as a compromise between the desirable compactness associated with a larger field, and the undesirable crowding or the extreme rays at the lower energy end towards the fringe region, which tends to occur less at smaller fields.

The design was optimized first, by using the TRANSPORT code.[5] By using the matrix method in six-dimensional phase space, this code maps both the horizontal and the vertical extent of the beam envelope along the central ray path. At the exit pole edge, the emerging ray bundles are focussed horizontally and defocussed vertically, resulting in lines images at the horizontal focus points. The latter lie along a nearly straight line. The width of the focal images is sensitive to a second order correction that is introduced by adding a small amount of curvature at the entrance pole edge. As the optimum, normalized curvature calculated from the matrix code was very closely realized by the inherent outwart bending of the field contours due to the finite width of the entrance pole edge,[6] the latter was machined flat but demountable for possible later rounding.

Because the matrix code calculates the extreme ray trajectories by means of a Taylor expansion about the central ray paths, the results become less accurate as the separation from the central ray increases. A raytracing code[7] therefore, was run to complement the matrix code results, making use of measured field data from the actual dipole magnet. Ray paths obtained from this code were used to draw the ray bundles shown in Fig. 1. The inner, central, and outer extreme rays do not generally intersect precisely at a common point; a perfect, triple intersection would imply a zero width focal image. It was verified graphically that the width of the raytracing, focal images was consistent with the 1 mm prediction from the matrix code. Because the focal lines predicted from the matrix and the raytracing codes were offset by a few millimeters, the detector plane was mounted so as to allow some back and forth motion for empirical adjustment, if required.

MECHANICAL DESIGN

The spectrograph magnet is an iron core dipole supplying a nominal 1000 Gauss field in a 2.0-cm wide gap. The pole piece shape, shown in Fig. 1, follows from the electron optics requirements, with the bulge along one side simulating a wide and symmetrical pole edge to the entering electrons. The magnetic circuit was designed using the 2-D finite element code JASON.[8] Magnetic saturation in the C1008 steel is avoided by holding the peak field to well under 8 kGauss. A Purcell gap is included between the yoke and the polepieces in order to equalize the flux distribution over the large pole area. Field clamps along the entry and exit pole edges provide good definition of the effective field boundary.

The coils are wound directly onto the polepieces, using 200 turns each of AWG 14 enameled copper wire. The wire was wound wet with a fixture filling the reentrant corner behind the entry edge bulge. After winding, the fixture was removed and a press was used to bend the entire coil cross-section along the polepiece contour before curing. Natural convection cooling is adequate as the power dissipation is approximately 50 W. Figure 2 shows the completed spectrograph.

Magnetic field measurements at the 0.1% level of accuracy were carried out with a Hall probe positioned to +/-0.5 mm by means of a three axis carriage.

The field resolution was 0.01 Gauss in a 1000 Gauss field. Before each measurement the magnet was conditioned by cycling slowly from zero to 1700 Gauss and back, thereby providing a repeatable magnetic history.

A perspective plot of the midplane field is shown in Fig. 3. Along a line through the center, and spanning the short dimension of the pole, the field was found to be constant within 0.05 percent. The same high degree of flatness was found along the entry pole edge over the central 5 cm of width, and along the exit pole edge over a width of 16 cm. Along the central line spanning the long dimension of the pole, we measured a linear, 0.5 percent increase of the midplane field towards the entry pole edge, probably due to the bulge in the pole face which decreases the reluctance of the magnetic circuit in that region. The effective field boundaries as derived from fringe field measurements, agreed with the calculated locations to within less than 0.5 mm.

The aluminum vacuum chamber is firmly aligned to the spectrograph magnet. The wall thickness under the poles is necessarily thin to accommodate a 1.2 cm inside clearance, but increases on the outside to provide stiffness. The detector plane is an aluminum bar coated with P1 phosphor, positioned with two micrometer driven, bellows sealed linear actuators. Fiducial marks are provided by backlighting two precisely located hole drilled through the bar. A second aluminum bar, plated with a 0.1 mm thickness of nickel and then lapped to a mirror finish, is placed near the detector screen so that the focal plane can be viewed through a 15-cm dia quartz viewport.

The dipole magnet, the vacuum chamber, and the quadrupole magnet (when used) are mounted and aligned together as a single system. The assembly is then placed on a positioning platform with cross-roller bearing slides and precision lead screws driven by stepper motors. A welded stainless steel bellows attached to the ELF beam tube allows the entire spectrograph assembly to be moved without breaking the vacuum. The spectrograph aperture can therefore be scanned across the electron beam both horizontally and vertically while the accelerator is in operation. Encoders attached to the lead screws allow positional accuracies of less than 0.1 mm.

SPECTROGRAPH CALIBRATION WITH A PROTON BEAM

In order to verify the raytracing results and to provide a working calibration of the instrument, an ion source was borrowed from Sandia Laboratories and activated. The apparatus is shown schematically in Fig. 4. There are three main parts to the system, each contributing its own errors to the calibration, i.e., the ion source, the spectrograph magnet, and the optical path for viewing the deflected beam.

The ion source is a Colutron Model G-2. Ionization of the source gas takes place through electron impact from a hot filament. After extraction through a pinhole aperture, the ions are accelerated to the desired beam potential, focused in an electrostatic lens, and passed through a Wien filter. However, the latter was not used during this calibration, as the spectrograph itself

provided adequate analysis of the donimant species, H+, H2+, and H3+, all of which provided calibration points. The emerging ion current (before collimation) was estimated at 10-20 microamperes. The accelerating potential was monitored with a Keithley Model 614 electrometer, through a Keithley Model 6103C, 1000:1, 5% high voltage probe. The Keithley system was calibrated against a Singer Metrics, electrostatic voltmeter, which in turn was compared to a standard differential voltmeter. The overall accuracy of the voltage measurement is estimated at 1-2% in the 3-5 kV range, and better than 0.5% above 5 kV.

The spectrograph magnet was excited with a laboratory power supply with 0.05% current regulation, and the current was monitored through a 10 milliohm, nominal 1% shunt. As this same shunt stayed with the instrument, the 1% uncertainty of the shunt resistance did not enter into the calibration. Before each data run, in order to forestall hysteresis errors, the magnet was carefully conditioned, and the operating point always was approached from below.

The ion beam enters the spectrograph through a 2 mm dia collimating aperture, and is bent and focused by the magnetic field into a line image of this aperature on the detector place. However, for weak beams, only the more intense, central portion of the line image remains visible. For purposes of this calibration, a Polaroid photograph of the detector plane, taken through a video camera and display unit, constituted the basic readout of the instrument. The scale factor for interpreting the photograph was established by scaling the distance between the two backlighted fiducial holes in the

detector plane, which are exactly 10 cm apart. Measurements were taken by changing the ion beam energy until the spot corresponding to the desired species (H+, H2+, or H3+) would show up somewhere between the two fiducial holes, then taking a photograph, and repeating this at a number of different energies. The width both of the beam spot and the fiducial spots on the photograph typically was 1 to 1.5 mm; note that a 2 mm dia collimator aperture was used for this calibration. The reading error in determining the beam spot position with a millimeter scale is conservatively estimated at 0.5 mm, or 1 or 2 percent, depending on the beam energy. This translates directly into an energy error, and it is probably the dominant error in this calibration. To reduce it, one would go to a smaller diameter beam sample and to smaller fiducial holes, and one would scan the photograph with a microdensitometer.

The original design of the spectrograph foresaw a quadrupole magnet preceding the spectrograph, for vertical prefocusing of the entering beam sample. However, during early measurements on the ELF experiment we found that good beam transmission to the detector plane was obtained even without the quadrupole, and the latter was thereafter left off. The ion source calibration also was done without the quadrupole. The conversion from ion energy to equivalent electron energy was made by invoking momentum equivalence between the two species. For example, a 4.5 to 9.5 keV proton energy range represents 2.4 to 3.8 MeV electrons. An absolute calibration, i.e., the energy reading referenced to the position of the fiducial holes, was obtained from the ion beam experiment for field values of 900, 1000, and 1100 Gauss, giving an execellent fit to a straight line in all cases. The dispersion found from the ion beam data is 12.6 kV/mm at 1000 Gauss, in good agreement with the value 13.3 kV/mm found from raytracing.

MEASUREMENT OF THE ELECTRON ENERGY DISTRIBUTION ON ELF

The electron spectrograph is mounted on the ELF beamline immediately following the interaction region, as shown schematically in Fig. 5. The waveguide for transporting the 34.6 GHz radiation from the interaction region to the diagnostic tank is offset from the beam axis in order to allow a straight trajectory for the electrons from the end of the wiggler to the spectrograph. This eliminates having to achromatically bend the electron beam into the spectrograph. The first mitre bend in the waveguide used a fine mesh screen that is transparent to the nominal 3.5 MeV electron beam, but reflective to the microwave signal. Beyond the screen, the electrons impinge on a 2 mm dia collimating aperture which extracts a several-Ampere sample from the 800 A beam. The phosphor-coated detector plane is viewed with a gated TV camera (10 ns gate) and the two-dimensional image is digitized and stored on disc for later analysis on a VAX 750 computer.

Fig. 6 shows three electron beam spectra and their corresponding densitometer traces, for three different values of wiggler magnetic field. In the top trace the wiggler field is 1.49 kG. This is far from the resonant field required for significant gain at 34.6 GHz, and hence the wiggler field only serves to transport the electron beam to the spectrograph without perturbing the electron distribution. In this trace the peak of the distribution occurs at 3.62 MeV, with a FWHM of 0.11 MeV (3% energy spread). Also, we see a small tail on the distribution extending towards lower energies. As the wiggler magnetic field is increased towards resonance (middle trace), the distribution

begins to spread to lower energies. In the bottom trace the wiggler field is at 3.4 kG and, although the peak of the distribution is at 3.61 MeV, the average electron energy is 3.49 MeV, i.e., the electron beam energy has been reduced by 3.2%. The spectrum shows two peaks in the distribution, one at 3.61 MeV and the other at 2.97 MeV. The average energy for this distribution is 3.18 MeV which corresponds to an overall reduction in electron energy of 12%.

These data are not inconsistent with the observed microwave output power levels; at 3.7 kG, the total, measured microwave power in the TE_{01}, TE_{21}, and TM_{21} modes was 250 MW. For a 3.61 Mev electron beam, this corresponds to an extraction efficiency of 9.3%, compared to 12% predicted from the spectrograph measurements. In the middle and bottom traces of Fig. 6 the fuducial markers were deleted and the signals normalized in order to show the structure of the distribution more clearly. There is no correlation between the amplitudes of the three traces.

In the spectra corresponding to FEL interaction there is some broadening toward higher energies. This is to be expected from the nature of the interaction: while most of the electrons have the appropriate phase to give energy to the electromagnetic wave, some electrons in the finite distribution are situated in phase so as to extract energy from the wave.

One difficulty encountered with measuring the spectrum of an electron beam with a broad energy distribution, is the transport of electrons from the end of the wiggler to the entrance of the spectrograph. It can be shown[9] that

the electron emerge from the wiggler with off-axis angles that depend on their energy. The low-energy electrons are most likely to miss the entrance aperture to the spectrograph, and this can result in an apparent distribution that is skewed towards the higher energies. We have no estimate of the magitude of this effect in our data, although we believe it to be small for the 10-to-20% shifts we are observing. We plan to address this problem in more detail, in order to take full advantage of the bandwidth of the spectrograph.

CONCLUSION

A wideband, 2-4 MeV magnetic spectrograph for use on the free-electron laser experiment at LLNL has been designed and built, and has been calibrated with a 2-6 keV proton beam. The measured dispersion is in good agreement with the value predicted from raytracing. The spectrograph has been used to estimate the extraction efficiencies achieved during FEL interaction with the electron beam. The results agree within 25% with the observed microwave power levels.

ACKNOWLEDGEMENTS

It is a pleasure to acknowledge many stimulating discussions with K. Halbach and A. C. Paul, concerning magnet design and raytracing. R. Kalibjian advised

us on the visual optics design, and W. J. Stearns provided much valuable expertise in completing the ion beam calibration work. Finally, the ELF data could not have been obtained without the dedicated effort of the ELF experimental crew, headed by J. Clark and A. Throop.

Figure Captions

1. Effective field boundaries and ray paths for the ELF spectrograph. For clarity, only the electron ray paths are shown. The adjustable detector plane is imaged in a mirror and viewed through an optical port (top right).

2. Photograph of spectrograph complete with vacuum chamber, adjustable detector plane, and optical port.

3. Perspective plot of the measured midplane field. The entry edge is shown at the top of the picture.

4. Schematic of ion beam calibration setup. For clarity, the mirror relaying the detector plane image to the camera is not shown.

5. Schematic of the ELF interaction region showing the method of mounting the spectrograph of the beamline. At the exit of the interaction region the microwaves are deflected out of the beam path with two mitre bends. The first reflector is a fine mesh screen which is transparent to the electron beam, allowing it to pass straight through to the spectrograph.

6. Spectral images and their densitometer traces for the electron beam after passing through the interaction region. The three traces correspond to three different values of wiggler field: (top) far off resonance, (middle) near resonance, (bottom) on resonance. In the middle and bottom traces the fiducial markers have been removed. The top trace indicates an initial electron beam energy of 3.62 MeV.

References

1. T. J. Orzechowski, E. T. Scharlemann, B. R. Anderson, V. K. Neil, W. M. Fawley, D. Prosnitz, S. M. Yarema, B. D. Hopkins, A. C. Paul, A. M. Sessler, and J. S. Wurtele, "High-Gain Free Electron Lasers Using Induction Linear Accelerators, "IEEE J. Quantum Electron, vol. QE-21, pp. 831-844, 1985.

2. R. C. Kennedy, J. L. Adamski, "Spectrograph for Free Electron Laser Experiments," Trans. IEEE NS-30 3142-3144 1983.

3. J. Borggren, B. Elbek, L. P. Nielson, "A Proposed Spectrograph for Heavy Particles," Nucl. Inst. Meth. 24 1-12 1963.

4. The use of an Elbek spectrograph of the ELF application was suggested to us by J. Pasour (NRL).

5. A. C. Paul, TRANSPORT, "An Ion Optic Program (LBL version)," LBL-2697,UC-32, Lawrence Berkeley Laboratory Feb. 1985.

6. H. A. Enge, "Deflecting Magnets, in Focusing of Charged Particles," A. Septier, ed., Vol. II, p. 262, Academic Press (1967).

7. A. C. Paul, "TRAJECTORY, An Orbit and Ion Optic Matrix Program for the 184 Inch Cyclotron," UCRL-19407, UC Lawrence Radiation Laboratory Sept. 1969.

8. S. Sackett, "JASON - A Code for Solving General Electrostatics Problems," User Manual, UCID-17814 June 1978.

9. A. C. Paul, unpublished work.

00281/00101

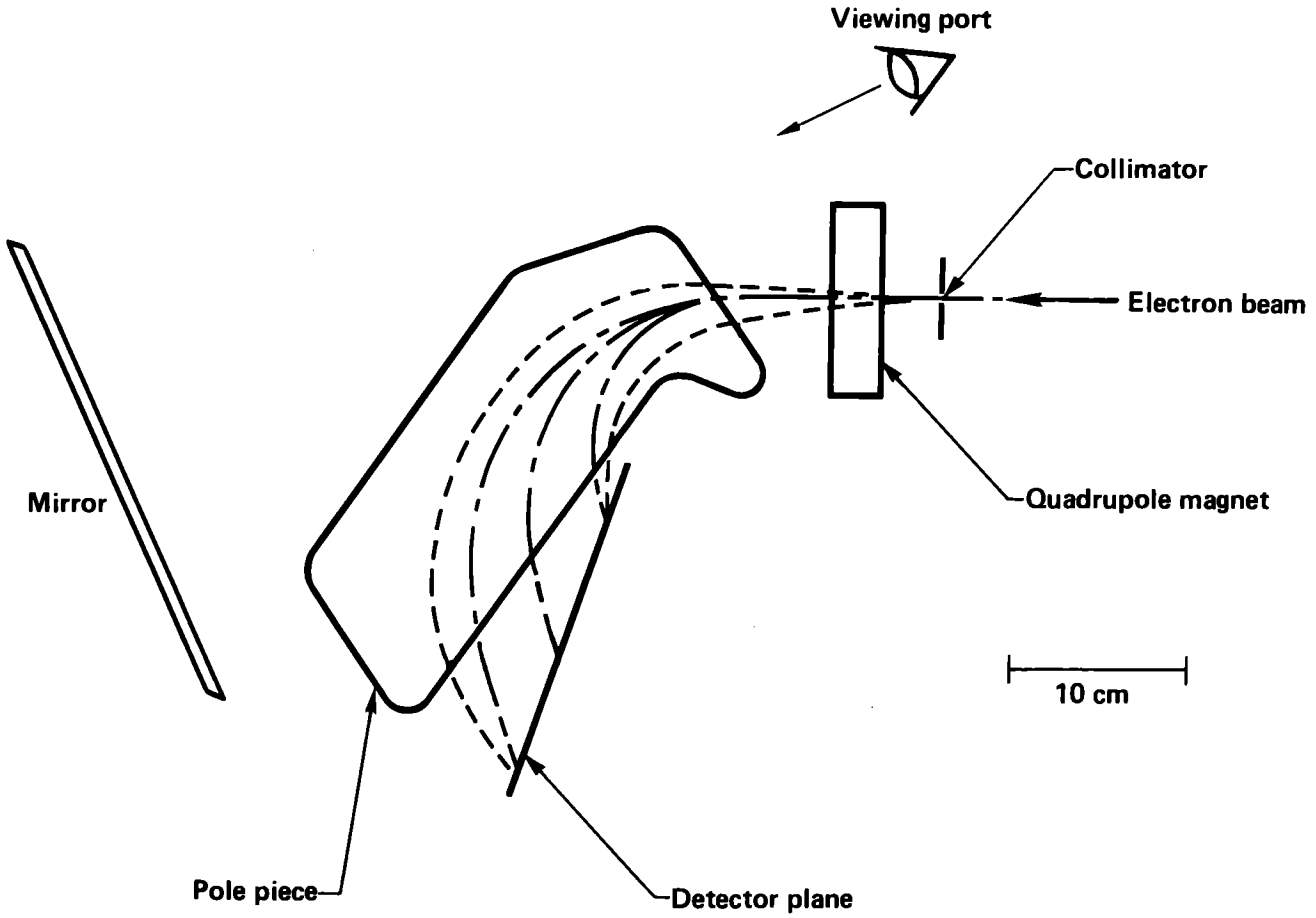
Viewing port
Collimator
Electron beam
Mirror
Quadrupole magnet
10 cm
Pole piece
Detector plane

Fig. 1

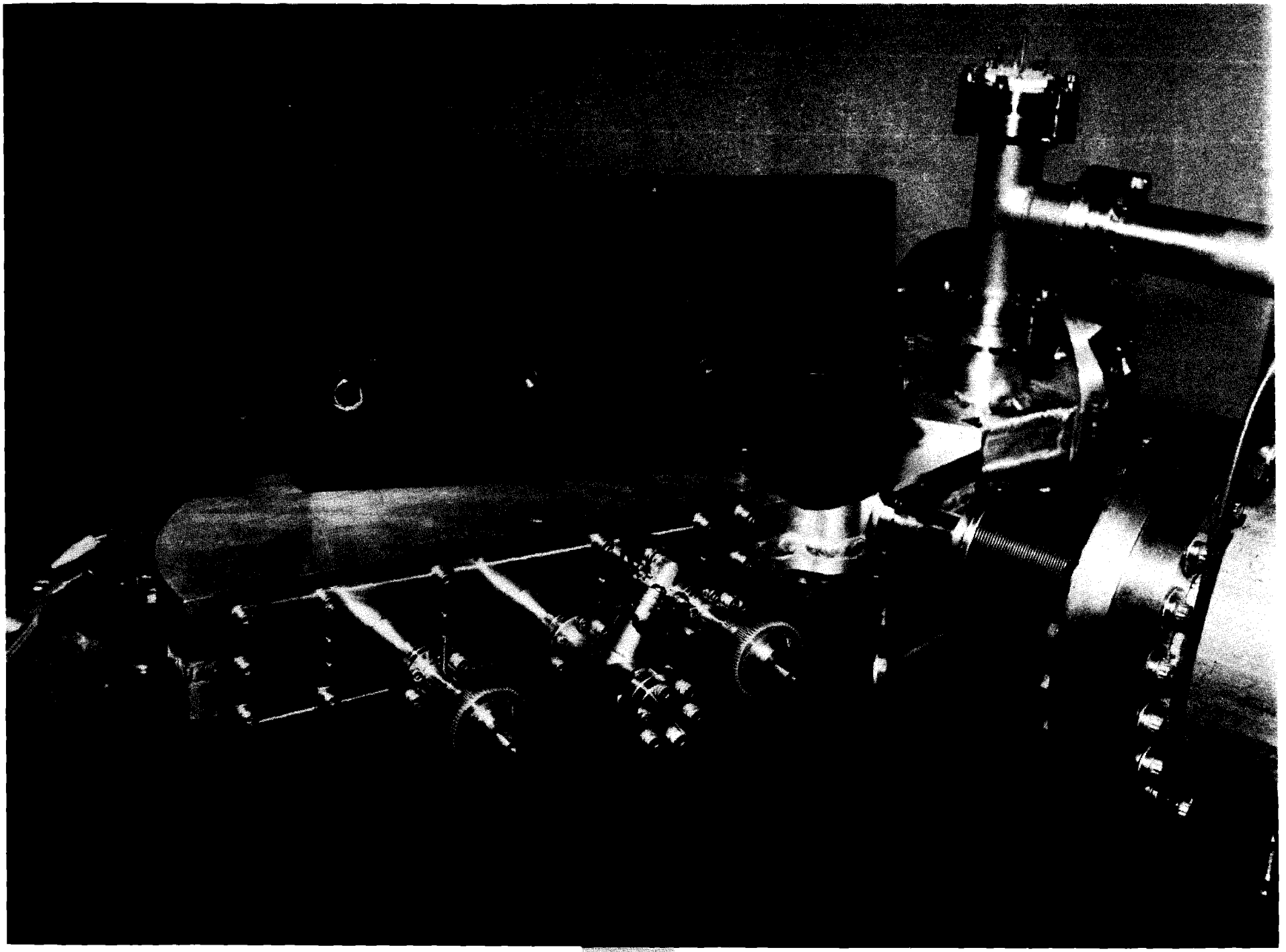

Fig. 2

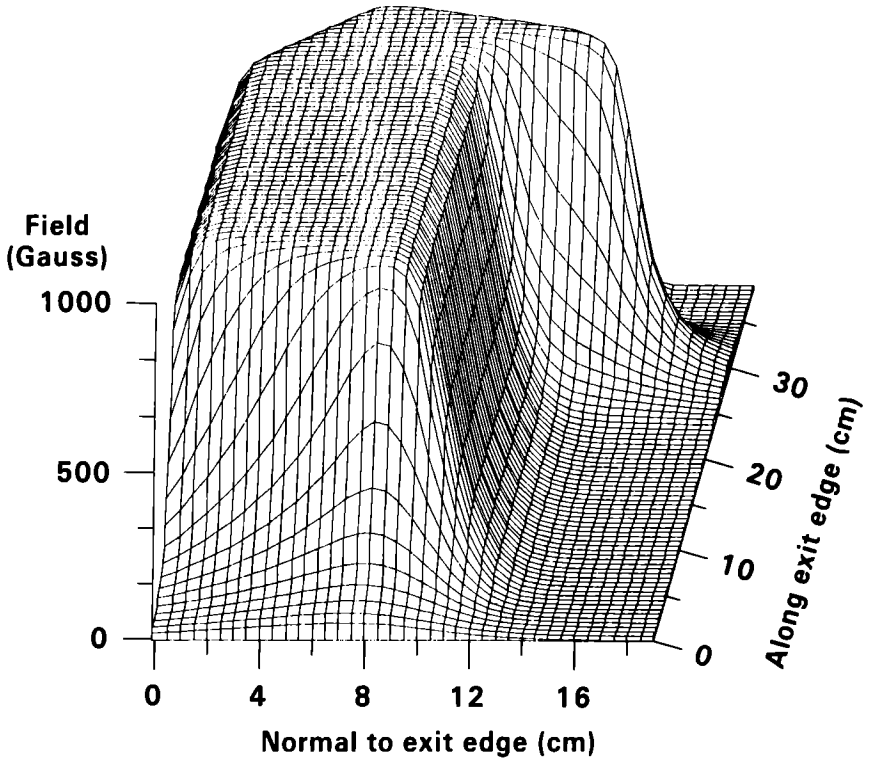
Field
(Gauss)
1000
500
0
0
4
8
12
16
Normal to exit edge (cm)
0
10
20
30
Along exit edge (cm)

Fig. 3

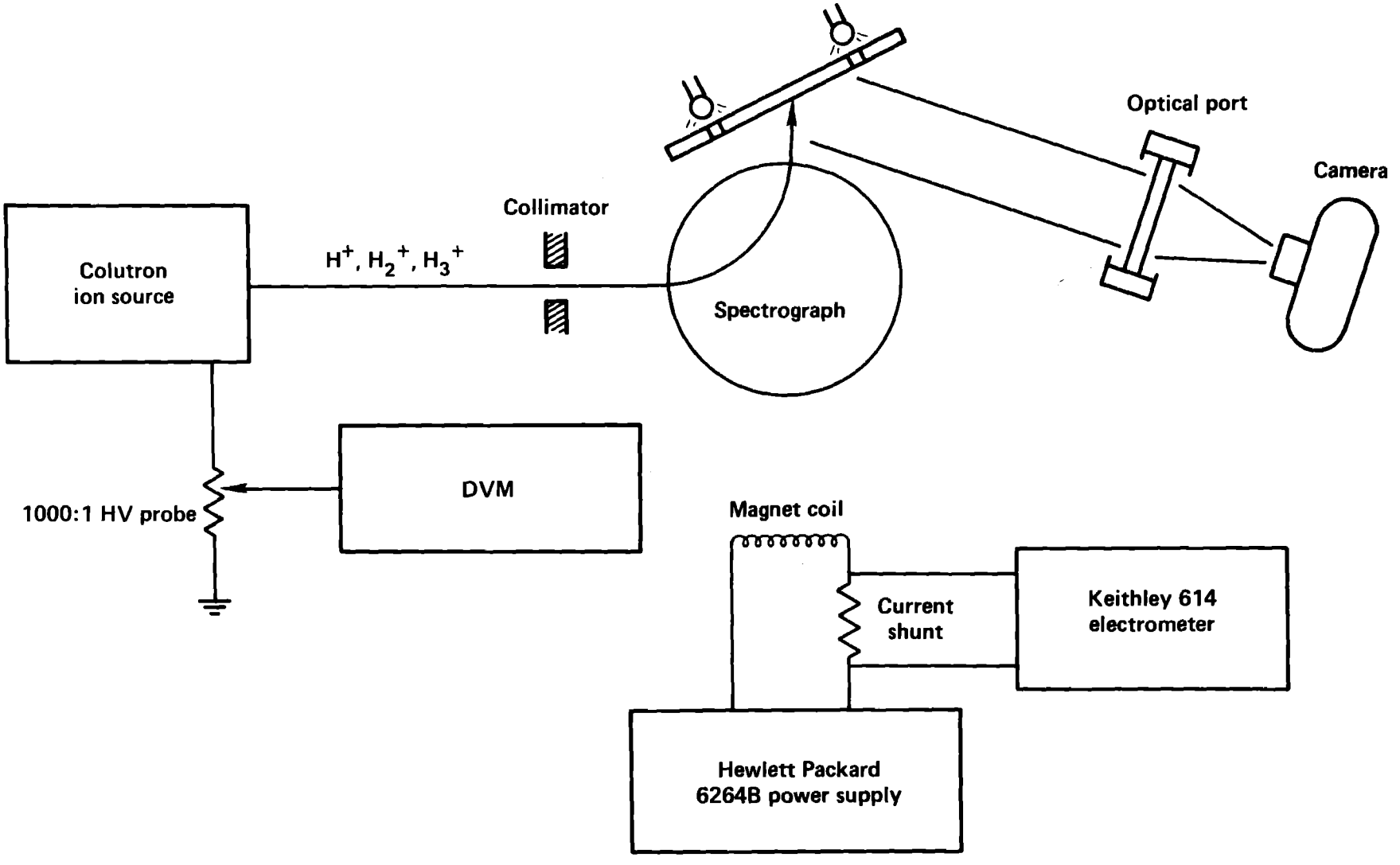
Optical port
Camera
Collimator
Colutron
ion source
H^+, H_2^+, H_3^+
Spectrograph
DVM
1000:1 HV probe
Magnet coil
Current
shunt
Keithley 614
electrometer
Hewlett Packard
6264B power supply

Fig. 4

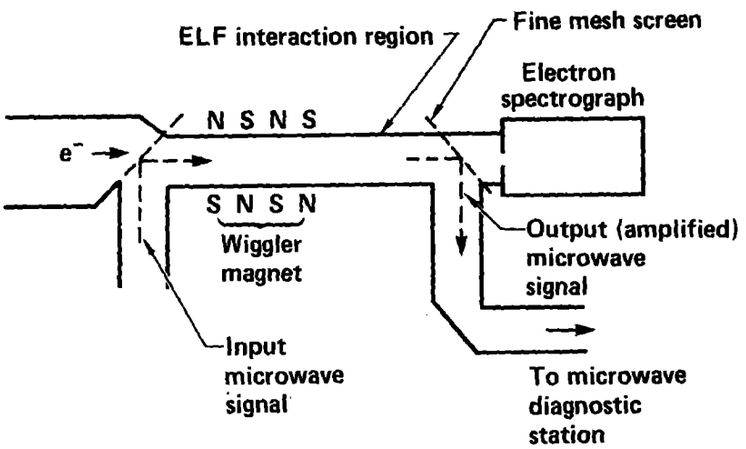
ELF interaction region
Fine mesh screen
Electron spectrograph
N S N S
e⁻
S N S N
Wiggler magnet
Output (amplified) microwave signal
Input microwave signal
To microwave diagnostic station

Fig. 5

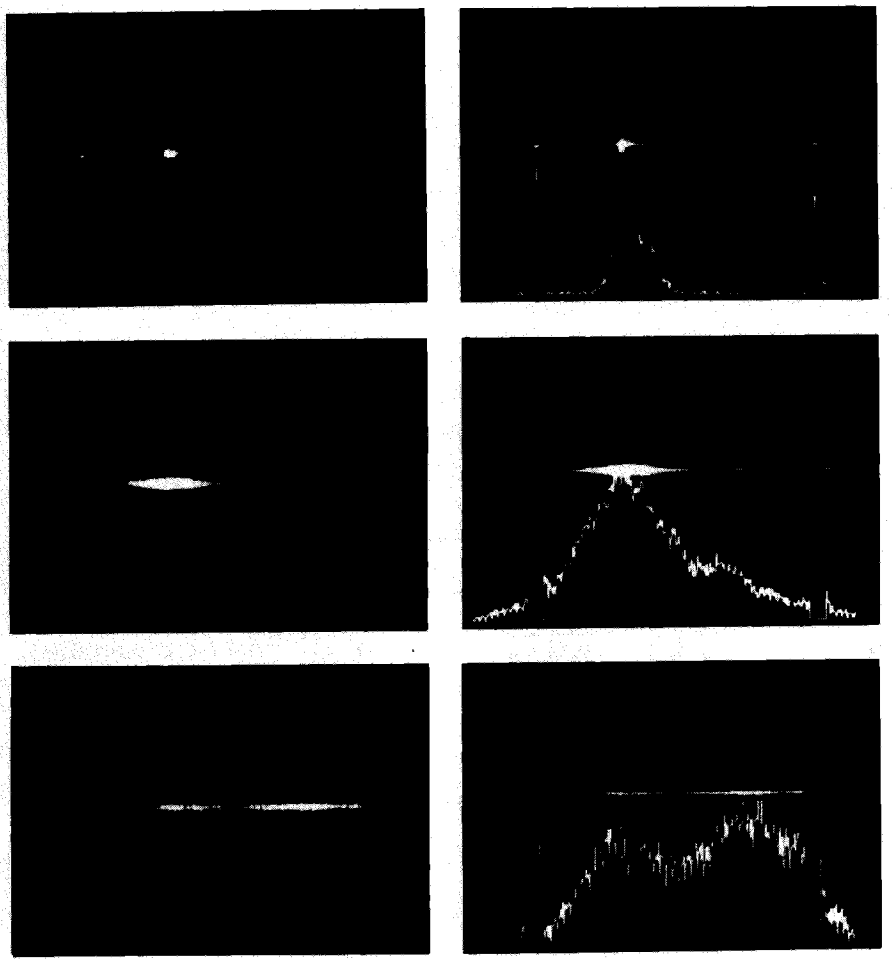

Fig. 6